

Chaos generation by a hybrid integrated chaotic semiconductor laser

Ming-Jiang Zhang(张明江), Ya-Nan Niu(牛亚楠), Tong Zhao(赵彤), Jian-Zhong Zhang(张建忠), Yi Liu(刘毅), Yu-Hang Xu(徐雨航), Jie Meng(孟洁), Yun-Cai Wang(王云才), An-Bang Wang(王安帮)
Citation: Chin. Phys. B . 2018, 27(5): 050502. **doi:** 10.1088/1674-1056/27/5/050502

Journal homepage: http://cpb.iphy.ac.cn; http://iopscience.iop.org/cpb

What follows is a list of articles you may be interested in

A new nonlinear oscillator with infinite number of coexisting hidden and self-excited attractors

Yan-Xia Tang(唐妍霞), Abdul Jalil M Khalaf, Karthikeyan Rajagopal, Viet-Thanh Pham, Sajad Jafari, Ye Tian(田野)
Chin. Phys. B . 2018, 27(4): 040502. **doi:** 10.1088/1674-1056/27/4/040502

A new four-dimensional chaotic system with first Lyapunov exponent of about 22, hyperbolic curve and circular paraboloid types of equilibria and its switching synchronization by an adaptive global integral sliding mode control

Jay Prakash Singh, Binoy Krishna Roy, Zhouchao Wei(魏周超)
Chin. Phys. B . 2018, 27(4): 040503. **doi:** 10.1088/1674-1056/27/4/040503

Effects of intrinsic and extrinsic noises on transposons kinetics

Alssadig A M Yousif, Lulu Lu(鹿露露), Mengyan Ge(葛梦炎), Ying Xu(徐莹), Ya Jia(贾亚)
Chin. Phys. B . 2018, 27(3): 030501. **doi:** 10.1088/1674-1056/27/3/030501

Generalized Chaplygin equations for nonholonomic systems on time scales

Shi-Xin Jin(金世欣), Yi Zhang(张毅)
Chin. Phys. B . 2018, 27(2): 020502. **doi:** 10.1088/1674-1056/27/2/020502

Topological horseshoe analysis and field-programmable gate array implementation of a fractional-order four-wing chaotic attractor

En-Zeng Dong(董恩增), Zhen Wang(王震), Xiao Yu(于晓), Zeng-Qiang Chen(陈增强), Zeng-Hui Wang(王增会)
Chin. Phys. B . 2018, 27(1): 010503. **doi:** 10.1088/1674-1056/27/1/010503

Chaos generation by a hybrid integrated chaotic semiconductor laser*

Ming-Jiang Zhang(张明江)[1,2,†], Ya-Nan Niu(牛亚楠)[1,2], Tong Zhao(赵彤)[1,2], Jian-Zhong Zhang(张建忠)[1,2], Yi Liu(刘毅)[1,2], Yu-Hang Xu(徐雨航)[1,2], Jie Meng(孟洁)[1,2], Yun-Cai Wang(王云才)[1,2], and An-Bang Wang(王安帮)[1,2,‡]

[1] *Key Laboratory of Advanced Transducers and Intelligent Control System, Ministry of Education and Shanxi Province, Taiyuan University of Technology, Taiyuan* 030024, *China*

[2] *Institute of Optoelectronic Engineering, College of Physics & Optoelectronics, Taiyuan University of Technology, Taiyuan* 030024, *China*

(Received 13 November 2017; revised manuscript received 6 February 2018; published online 26 April 2018)

We design a hybrid integrated chaotic semiconductor laser with short-cavity optical feedback. It can be assembled in a commercial butterfly shell with just three micro-lenses. One of them is coated by a transflective film to provide the optical feedback for chaos generation while insuring regular laser transmission. We prove the feasibility of the chaos generation in this compact structure and provide critical external parameters for the fabrication by theoretical simulations. Rather than the usual changeless internal parameters used in previous simulation research, we extract the real parameters of the chip by experiment. Moreover, the maps of the largest Lyapunov exponent with varying bias current and feedback intensity K_{ap} demonstrate the dynamic characteristics under different external-cavity conditions. Each laser chip has its own optimal external cavity length (L) and feedback intensity (K_{ap}) to generate chaos because of the different internal parameters. We have acquired two ranges of optimal parameters ($L = 4$ mm, $0.12 < K_{ap} < 0.2$ and $L = 5$ mm, $0.07 < K_{ap} < 0.12$) for two different chips.

Keywords: chaotic dynamic characteristics, integrated chaotic semiconductor laser, short-cavity optical feedback, extraction of internal parameters

PACS: 05.45.–a, 42.82.–m, 42.55.Px **DOI:** 10.1088/1674-1056/27/5/050502

1. Introduction

Chaos has attracted considerable research interest because of its many potential applications, such as secure communication,[1,2] high-speed random number generation,[3–5] chaotic radar,[6–8] optical fiber detection,[9–11] weak signal detection[12,13] and distributed optical sensors.[14–18] Semiconductor lasers can easily generate chaos[19] with additional degrees of freedom, such as optical feedback, optical injection, electro-optical feedback and mutual coupling.[20–24] Nowadays, most chaotic lasers are fabricated by using discrete optical components in a laboratory. However, such chaotic lasers are bulky and easily affected by the external environment, which is not conducive to their practical application and large-scale production.[25–27] To solve these problems, many research groups have put forward the integrated chaotic semiconductor laser.

Recently, some monolithic integrated chaotic semiconductor laser chips have been reported. A laser chip with optical feedback was developed by Satoshi Sunada *et al.,*[28] which consists of a distributed feedback laser (DFB), two semiconductor optical amplifiers, a photodiode and a passive ring waveguide cavity. The chaos with a flatness of ±6.5 dB and a bandwidth of 10 GHz was obtained. Wu *et al.* also proposed a laser chip,[27] which includes a DFB section, a phase section, an amplification section and a high-reflection coating to the face of the amplifier section. The chaotic bandwidth increased to more than 26.5 GHz when using this monolithic integrated structure. Yin *et al.* researched the generation of wideband chaotic signal and generated a chaotic signal of 36 GHz by using a three-section monolithic integrated semiconductor laser under external optical injection.[29] The development of monolithic integrated chaotic semiconductor laser chips has reduced the size of the chaotic lasers and improved the quality of the chaotic signal. However, the production of monolithic integrated chaotic semiconductor laser chips requires sophisticated and expensive instruments, and every step of the growth process must be strictly controlled, which restricts the mass production of monolithic integrated chaotic semiconductor lasers.

Therefore, it is necessary to design a new simple integrated chaotic laser. The feasibility verification of the structure through numerical simulation is an indispensable step in the design process. In the structure that produces chaos, the short cavity optical feedback structure is easiest to integrate.[30]

*Project supported by the International Science and Technology Cooperation Program of China (Grant No. 2014DFA50870), the National Natural Science Foundation of China (Grant Nos. 61377089, 61475111, and 61527819), Shanxi Province Natural Science Foundation, China (Grant No. 2015011049), Shanxi Province Youth Science and Technology Foundation, China (Grant No. 201601D021069), Shanxi Scholarship Council of China (Grant No. 2016-036), Program for the Outstanding Innovative Teams of Higher Learning Institutions of Shanxi, China, and Program for Sanjin Scholar, China.

†Corresponding author. E-mail: zhangmingjiang@tyut.edu.cn

‡Corresponding author. E-mail: wanganbang@tyut.edu.cn

© 2018 Chinese Physical Society and IOP Publishing Ltd

However, it is very sensitive to the external cavity length and the feedback intensity required for the generation of chaos.[31] A small change of the external conditions may have a significant effect on the dynamic characteristics of this structure. Due to the different internal parameters of different laser chips, the length of the external cavity and the feedback intensity are different. This makes previous simulation methods no longer applicable. And we should utilize real internal parameters in the numerical simulation to ensure that the designed integrated chaotic laser can generate chaos.

In this paper, we propose an easy-to-implement hybrid integrated chaotic semiconductor laser with a short external feedback cavity. The frequency test method of the network analyzer is used for acquiring the internal parameters of the chaotic semiconductor laser chip 1 (CSLC1) and CSLC2, and the extracted parameters are used for the following simulation. We obtain the optimal external cavity length and the optimal feedback intensity for the generation of chaos, corresponding to the different internal parameters of each chip. In addition, the results provide a theoretical foundation for the production of the hybrid integrated chaotic semiconductor lasers.

2. Structural design

2.1. Integrated structure

The structural design is based on the theory of a standard single-mode semiconductor laser subject to external optical feedback. The schematic diagram of the hybrid integrated semiconductor laser is shown in Fig. 1, which consists of a semiconductor laser section, a collimating lens, a transflective mirror and a focusing lens, with lengths of 0.3 mm, 1.0 mm, 1.0 mm and 1.5 mm, respectively. A semiconductor laser chip is stuck to the sub-mount. The optical fiber is fixed by a Ω hold. All the sections above are fixed on a heat sink. A semi-reflective film is coated on one side of the transflective mirror. The parts between the transflective mirror and the front face of the semiconductor laser chip work as an external feedback cavity. The length of the external cavity is in the range of 2 mm to 6 mm. The strength of the optical feedback is controlled by the reflectivity of the transflective film. The end of the optical fiber is coated with an antireflection film to avoid the additional reflection from the end of the optical fiber.

The semiconductor laser chip emits continuous light, which is collimated by the collimating lens and is divided into two parts by the transflective mirror. One part is coupled to the optical fiber, and the other part is reflected to the laser active resonator cavity. The chaotic light is generated by the optical feedback and is finally output by the optical fiber.

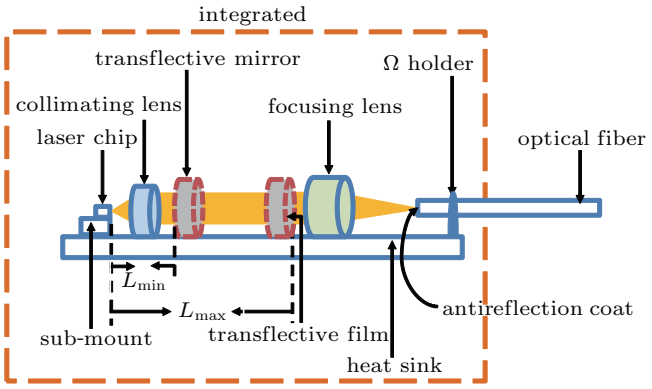


Fig. 1. (color online) Schematic diagram of the hybrid integrated chaotic semiconductor laser.

2.2. Rate equation model

In theory, the laser active resonator cavity is called the internal cavity, and the structure between the front face of the semiconductor laser chip and the transflective mirror is defined as the external cavity. The chaotic generation with optical feedback can be expressed by the Lang–Kobayashi equations.[32] The equations for the electric field amplitude $E(t)$, the carrier density $N(t)$ and the electric field phase $\varphi(t)$ are, respectively,

$$\frac{\mathrm{d}E(t)}{\mathrm{d}t} = \frac{1}{2}\left[\frac{\Gamma g_0 [N(t)-N_0]}{1+\varepsilon E^2(t)} - \frac{1}{\tau_\mathrm{p}}\right] E(t) + \frac{K_\mathrm{ap}}{\tau_\mathrm{in}} E(t-\tau_t)\cos\theta(t), \tag{1}$$

$$\frac{\mathrm{d}N(t)}{\mathrm{d}t} = \frac{I(t)}{qV_\mathrm{act}} - \frac{N(t)}{\tau_\mathrm{c}} - \frac{g_0 [N(t)-N_0]}{1+\varepsilon E^2(t)} E^2(t), \tag{2}$$

$$\frac{\mathrm{d}\phi(t)}{\mathrm{d}t} = \frac{\alpha}{2}\left[\frac{\Gamma g_0 [N(t)-N_0]}{1+\varepsilon E^2(t)} - \frac{1}{\tau_\mathrm{p}}\right] - \frac{K_\mathrm{ap}}{\tau_\mathrm{in}} \frac{E(t-\tau_t)}{E(t)} \sin\theta(t). \tag{3}$$

In Eq. (1), $K_\mathrm{ap} = (1-R_2)\times(R_\mathrm{ext}/R_2)^{1/2}$ represents the effect of the time-delay optical feedback, which also holds for the phase equation of Eq. (3). The intensity reflectivity at the front facet of CSLC is $R_2 = 0.3$ and R_ext represents the intensity reflectivity of the transflective film. In addition, the second term of Eq. (1) includes τ_in, $\theta(t)$ and τ_t. The round-trip time in the internal cavity is $\tau_\mathrm{in} = 7.1\times10^{-12}$ s. The round-trip time of feedback light in the external cavity is defined as $\tau_t = (2n_\mathrm{ext}L)/C$, where L is the external cavity length, n_ext is the refractive index of the external cavity and C is the velocity of light. The external cavity consists of two parts, the collimating lens and the nitrogen part. The refractive index and the length of the collimating lens are set to 1.6 and 1 mm, respectively. The refractive index of nitrogen is set to 1 and the length is a variable. $\theta(t) = \omega\tau_t + \varphi(t) - \varphi(t-\tau_t)$ represents the optical feedback phase, where ω is the angular frequency of the solitary laser chip and φ is the electric

field phase; the same argument holds for the phase equation of Eq. (3). The first right-side term of Eq. (2) includes V_{act} and q. $V_{act} = 4.8 \times 10^{-18}$ m^3 is the active volume of the semiconductor laser chip and $q = 1.602 \times 10^{-19}$ C is the electron charge.

The internal parameters of the CSLCs that need to be known in Eqs. (1)–(3) are defined as follows: Γ is the field confinement factor, g_0 is the differential gain, N_0 is the carrier density at transparency, τ_p is the photon lifetime, ε is the gain saturation coefficient, τ_c is the carrier lifetime and α is the line width enhancement factor. It is worth noting that the internal parameters are associated with parameters such as relaxation oscillation frequency, damping factor and threshold current. Accurate extraction of the internal parameters is crucial to selecting the optimized external cavity length and external reflection intensity.

The external cavity frequency is defined as $f_{ext} = 1/\tau_t$. A system can be classified as either short-cavity (when external cavity frequency f_{ext} is larger than relaxation oscillation frequency f_r) or long-cavity (when f_{ext} is less than f_r[33]). The long-cavity structure is longer than the commercial butterfly shell, unable to be integrated into the shell. Thereupon we design a short-cavity structure.

The aim of the simulation is to obtain accurate external cavity length L and feedback intensity K_{ap}, and ensure that the fabricated chaotic laser can produce chaos. However, the short-cavity structure is very sensitive to the external cavity length and the feedback intensity. Due to the different internal parameters of different laser chips, the length of the external cavity and the feedback intensity are different. We should utilize real internal parameters in the numerical simulation to ensure that the designed integrated chaotic laser can generate chaos. Therefore, we must extract the internal parameters of the chips.

3. Extraction of the internal parameters

By measuring the P–I curve and the small signal frequency response curve of the CSLC, we can obtain the threshold current, relaxation oscillation frequency and damping factor. These three parameters will be used in the subsequent internal parameter calculation.

The steady-state laser output power versus bias current relationship has been established as

$$P = \frac{I - I_{th} - I_S + \sqrt{(I - I_{th} - I_S)^2 + 4I_S I}}{2F}. \tag{4}$$

By fitting, we can obtain the I_{th} and the leaky current I_S. The I_{th} is equal to $(qv_{act}N_{th})/\tau_c$, and the I_S is equal to $[\Gamma\tau_p(I - I_{th})]/(qv_{act})$.

The experimental setup of the small signal intensity modulated frequency response curve is shown in Fig. 2, the low-cost laser diode driver (ILX Lightwave, LDX3412) and the vector network analyzer (ROHDE & SCHWARZ, ZVA24, 10 MHz–24 GHz bandwidth) provide direct current and radio frequency signals, respectively. The two signals mixed by a bias-T which is fixed on the vector network analyzer. The two signals are supplied to the CSLC by a high-frequency probe (Cascade Microtech, ACP40-GS-200, DC to 40 GHz).

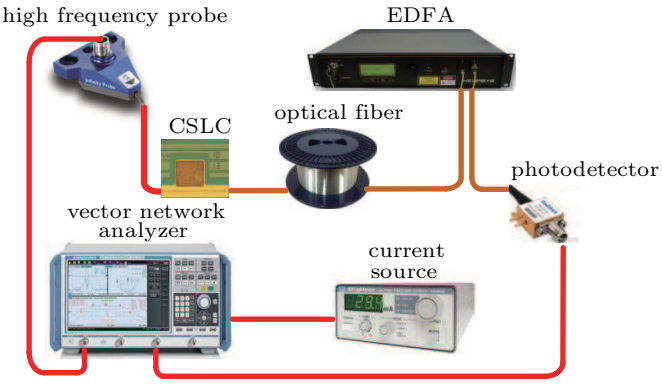


Fig. 2. (color online) Experimental device diagram for measuring frequency responses. The optical fiber and EDFA are used only to measure the fiber frequency response.

CSLC1 emits continuous light which is converted into an electrical signal by a photodetector (Finisar, XPDV2120RA, 50 GHz bandwidth). Then, the electrical signal is measured by the vector network analyzer. The measured result is the laser frequency response curve, as shown in Fig. 3(a).

The relative frequency response curves can be obtained by subtracting the frequency response at a lower biased current from the ones biased at higher biased current, as shown in Fig. 3(b). The method of the frequency response subtraction can eliminate all the adverse effects that are caused by the equipment and do not vary with the bias current during the experiment. The relative frequency response curves satisfy

$$P = 20\log_{10}\left(\frac{f_{r2}^2\sqrt{\left(f_{r1}^2 - x^2\right)^2 + \left(\frac{v_1 x}{2\pi}\right)^2}}{f_{r1}^2\sqrt{\left(f_{r2}^2 - x^2\right)^2 + \left(\frac{v_2 x}{2\pi}\right)^2}}\right), \tag{5}$$

where f_{r1}, f_{r2} and v_1, v_2 are the relaxation oscillation frequencies and the damping factors at the lower bias level and some higher level, respectively. By fitting, the relaxation oscillation frequencies and damping factors for different bias currents can be obtained. The $(2\pi f_r)^2$ is equal to $(\Gamma g_0)/(qv_{act})$ and the v is equal to $(1/\tau_c + Kf_r^2)$.

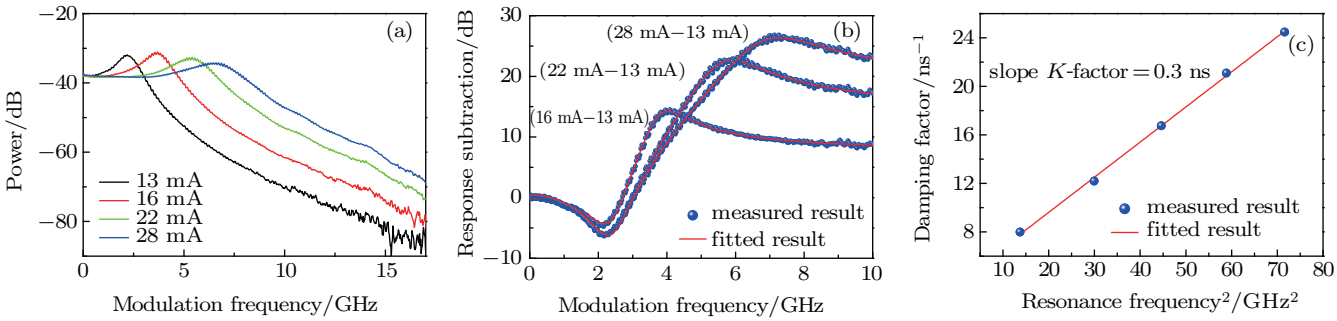


Fig. 3. (color online) (a) The laser frequency responses of CSLC1 for different bias currents. (b) Fitted results when the laser frequency response of 13 mA is subtracted from the laser frequency response for other higher bias currents. (c) Damping factor versus the relaxation oscillation frequency squared (the slope gives a value of 0.3 ns for *K*-factor).

Figure 3(a) shows the results of the laser frequency response curves when the bias current is 13 mA, 16 mA, 22 mA and 28 mA. Figure 3(b) depicts the fitted results of CSLC1 relative to the response of 13 mA biased current. The blue curves represent the measured results and the red curves are the fitted results.

The relaxation oscillation frequency squared versus the damping factor is linear, as shown in Fig. 3(c). The slope of the line is the *K*-factor[34] of 0.3 ns. The *K*-factor is equal to $[4\pi^2(\tau_p + \tau_n)]$.

The threshold current I_{th} of CSLC1 is 11.3 mA. The active volume V_{act} of the laser chip is provided. The two values, together with the measured values (f_r, v and *K*-factor), can be used to calculate the carrier lifetime τ_c and the threshold carrier density N_{th} of CSLC1 according to the reported calculation methods.[35–37]

The light-wave signal generated by CSLC is coupled into the dispersive optical fiber and amplified by an erbium doped optical fiber amplifier (EDFA, KEOPSYS, CEFA-C-HG). The amplified signal is converted into an electrical signal by a photodetector. Finally, the electrical signal is tested by the vector network analyzer. The electrical signal is the fiber frequency response.

The fiber frequency responses use the absolute value on the logarithmic domain with subtraction of the laser frequency response at the same bias current. The obtained curves fit to

$$P = 20\log_{10}\left(\sqrt{\cos^2\left[(2\pi x)^2 F_D\right] - \alpha\sin\left[2(2\pi x)^2 F_D\right] + \alpha^2\left(\frac{f_c^2}{x^2}+1\right)\sin^2\left[(2\pi x)^2 F_D\right]}\right), \tag{6}$$

where α and f_c are the line width enhancement factor and the chirp frequency, respectively. The f_c is equal to $(2\pi\tau_n f_r^2)$. The F_D is a parameter that indicates the attenuation characteristics of the optical fiber.

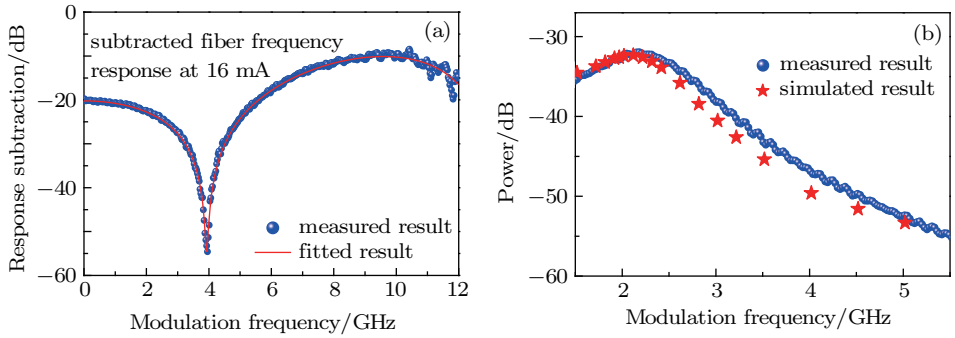


Fig. 4. (color online) (a) Fiber frequency response subtracts the laser frequency response at 16 mA. (b) Result of simulated laser frequency response (red star) at 13 mA and the measured laser frequency response (blue ball) at the same bias current.

The fitted results of the fiber frequency responses of CSLC1 are shown in Fig. 4(a). The blue and red curves represent the measured and the fitted results at 16 mA, respectively. The values of α and f_c together with the measured values above can be used to calculate the internal parameters (N_0, τ_p, g_0, Γ and ε) of CSLC1. Then all the internal parameters of CSLC1 can be extracted by the experiment, which are listed in Table 1.

To verify the accuracy of the parameters, we compare the laser frequency response of calculation and experiment at the same bias current, as shown in Fig. 4(b). At the bias current of 13 mA, we use the extracted parameters to simulate the laser frequency response which is represented by the red star. The experimental results deviate slightly from the simulation results due to the systematic errors in the experimental system. The systematic errors are mainly caused by the frequency re-

sponse nonuniformity of the electric adapter and cable. However, the internal parameters used in the simulation are obtained after eliminating the systematic errors, so the simulation result is accurate. Then, we utilize the extracted internal parameters for the following design.

Table 1. Internal parameters of CSLC1.

Parameter	Value
Threshold current I_{th}/mA	11.3
Wavelength λ/nm	1550
Linewidth enhancement factor α	3.04
Threshold carrier density N_{th}/m^{-3}	2.943×10^{24}
Carrier density at transparency N_0/m^{-3}	0.905×10^{24}
Photon lifetime τ_p/s	5.2×10^{-12}
Carrier lifetime τ_c/s	0.2×10^{-9}
Field confinement factor Γ	0.01
Differential gain g_0/m$^3\cdot$s^{-1}	9.434×10^{-12}
Gain saturation coefficient ε/m^3	2.271×10^{-23}
Round-trip time in internal cavity τ_{in}/s	7.1×10^{-12}
Active volume V_{act}/m^3	4.8×10^{-18}

Furthermore, we extract the internal parameters of CSLC2 by experiment, which are listed in Table 2. We also utilize the internal parameters of CSLC2 for the rate equations, and investigate its dynamic characteristics.

Table 2. Internal parameters of CSLC2.

Parameter	Value
Threshold current I_{th}/mA	11.4
Wavelength λ/nm	1550
Linewidth enhancement factor α	3.85
Threshold carrier density N_{th}/m^{-3}	3.8×10^{24}
Carrier density at transparency N_0/m^{-3}	0.16×10^{24}
Photon lifetime τ_p/s	5.2×10^{-12}
Carrier lifetime τ_c/s	0.256×10^{-9}
Field confinement factor Γ	0.01
Differential gain g_0/m$^3\cdot$s^{-1}	5.28×10^{-12}
Gain saturation coefficient ε/m^3	3.938×10^{-23}
Round-trip time in internal cavity τ_{in}/s	7.1×10^{-12}
Active volume V_{act}/m^3	4.8×10^{-18}

4. Results and discussion

To obtain an insight into the route to chaos of the system, we present the bifurcation diagram of CSLC1 for $I = 2.2I_{th}$ and $L = 4$ mm in Fig. 5. The feedback strength K_{ap} is taken as the variable. It is shown that the system experiences steady state (A), one-period oscillation (B), two-period oscillation (C), four-period oscillation (D), eight-period oscillation (E), and finally into the chaotic state.

Figure 6 describes the dynamic characteristics of CSLC1 in the time domain and frequency domain, the columns from (I) to (III) plot the time series, the optical spectra and the frequency spectra operated at different state, respectively. The bias current and the external cavity are set at $I = 2.2I_{th}$ and $L = 4$ mm for all cases. The values of I and L are optimized by the simulation. The external cavity frequency is $f_{ext} = 1/\tau_t = 32.6$ GHz, and the relaxation oscillation frequency is $f_r = 6.2$ GHz, corresponding to a short cavity with $f_{ext}/f_r > 5.2$.

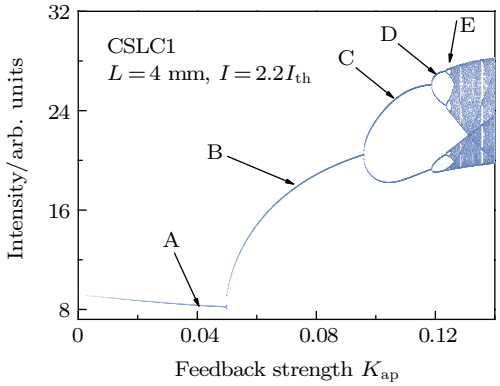


Fig. 5. (color online) Bifurcation diagrams of CSLC1: steady state (A), one-period oscillation (B), two-period oscillation (C), four-period oscillation (D), eight-period oscillation (E).

Figure 6(a) (the first row) is the case with feedback intensity $K_{ap} = 0.015$. It can be seen from Fig. 6(a-I) that the output power is constant. The optical spectrum (Fig. 6(a-II)) shows a typical single mode shape without deviation. The power of the frequency spectrum reflected in Fig. 6(a-III) is very low. These indicate that the laser oscillation is damped and the dynamics of the system is steady state.

As K_{ap} increases from 0.015 to 0.07, the laser appears non-damped oscillations and the system enters the one-period oscillation. As shown in Fig. 6(b-I), the laser shows an uniform pulsation with period of $1/f_{po}$, it has only one peak. The optical spectrum (Fig. 6(b-II)) shows peaks at $f_{po} = 7.68$ GHz and $2f_{po}$. The frequency spectrum (Fig. 6(b-III)) shows peaks at f_{po}, $2f_{po}$, $3f_{po}$ and $4f_{po}$, where $2f_{po}$, $3f_{po}$ and $4f_{po}$ are higher harmonics of the laser. The sharp peak f_{po} is not necessarily equal to the relaxation oscillation frequency f_r, only close to it.

Figure 6(c) (the third row) shows different dynamics when K_{ap} increases to 0.11. As can be seen from Fig. 6(c-I), the laser output shows two peaks of different heights with period of $1/\nu_e$. The optical spectrum (Fig. 6(c-II)) and frequency spectrum (Fig. 6(c-III)) are characterized by two sharp peaks at $f_{po} = 7.38$ GHz and ν_e (ν_e is its half-harmonic $f_{po}/2$).[38,39] These correspond to the double-period state.

The dynamics of CSLC1 at $K_{ap} = 0.16$ are shown in Fig. 6(d) (the fourth row), which is more complicated and can be called the chaotic state. The chaotic state is characterized by irregular time variations and larger amplitudes, as shown in Fig. 6(d-I). The optical spectrum (Fig. 6(d-II)) and frequency spectrum (Fig. 6(d-III)) are continuous. It is visible that the frequency spectrum covers a broad frequency range with a sharp peak f_{po} at 6.97 GHz.

Figure 6 plots the typical examples of the period-doubling route to chaos. Moreover, the peak frequency f_{po} decreases with the increase of K_{ap}.[39]

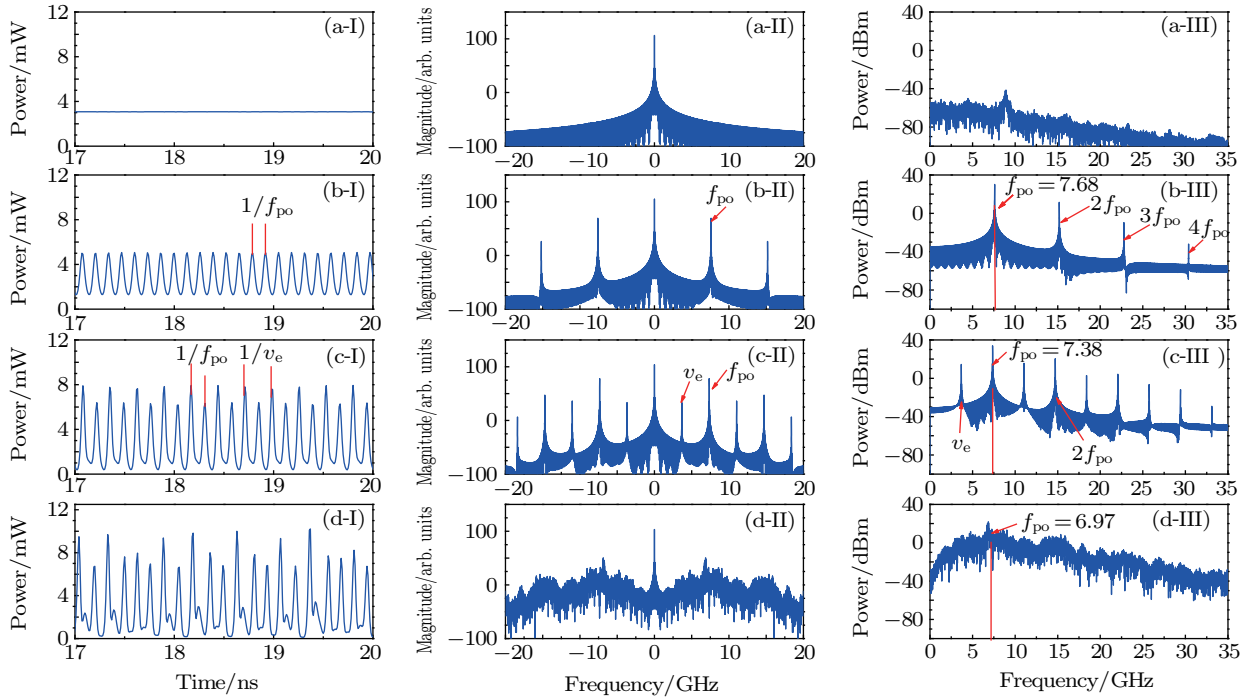


Fig. 6. (color online) Calculated time series (I), optical spectra (II), and frequency spectra (III) of the chaotic semiconductor laser chip 1: (a) the steady state, $K_{ap}=0.015$; (b) the one-period oscillation, $K_{ap}=0.07$; (c) two-period oscillation, $K_{ap}=0.11$; (d) chaotic state, $K_{ap}=0.16$. The bias current is $I=2.2I_{th}$ and the short external cavity length is $L=4$ mm.

The numerical result of the largest Lyapunov exponent of CSLC1 is shown in Fig. 7, the length of the feedback cavity L is 4 mm and the current I is $2.2I_{th}$. If the largest Lyapunov exponent is positive,[40] it indicates that the system is in the chaotic state. The largest Lyapunov exponent is negative or close to zero for the regions of the steady-state and periodic oscillations. It can be seen from Fig. 7, when the feedback strength is less than 0.04, the largest Lyapunov exponent is less than 0, the system is in the steady state; $0.04<K_{ap}<0.12$, the largest Lyapunov exponent is around 0 and the system is in the periodic state; when the feedback strength is greater than 0.125, the largest Lyapunov exponent is larger than 0, and thus the system is in the chaotic state.

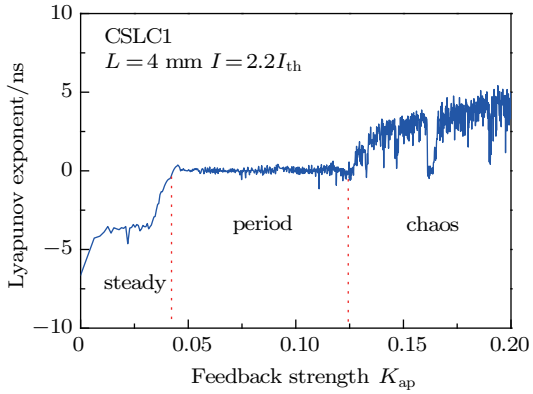


Fig. 7. (color online) Largest Lyapunov exponent as a function of the feedback strength K_{ap} of CSLC1. Feedback cavity L is 4 mm and bias current I is $2.2I_{th}$.

To investigate the comprehensive effects of bias current (15–41 mA) and K_{ap} (0–0.2) on CSLC1, we apply the maps of the largest Lyapunov exponent to estimate the dynamics of this system under different external cavities,[40] as shown in Fig. 8. Different colors in the dynamic maps represent different values of the largest Lyapunov exponent. When the Lyapunov exponent is far less than zero, it is expressed in blue; near zero in green; and greater than zero with red and yellow. As shown in Figs. 8(a) and 8(b), when the external cavity $L=2$ mm and $L=3$ mm, the largest Lyapunov exponent is far less than 0, which corresponds to the steady state of CSLC1.

When the external cavity length is equal to 4 mm, the result is shown in Fig. 8(c). Figure 8(c) indicates that the largest Lyapunov exponent remains negative when optical feedback $K_{ap}<0.12$. Among them, K_{ap} is <0.04 and the bias current ranges from 15 mA to 41 mA, the system is in a steady state, which is represented in blue; $0.04<K_{ap}<0.12$ and the bias current increases from 15 mA to 41 mA, the system is in the period-doubling state, which is marked by green. Only when $0.12<K_{ap}<0.2$ and the bias current increases from 22 mA to 41 mA, CSLC1 can generate chaos which is marked by yellow and red.

When the external-cavity length increases to 5 mm, the chaotic state disappears and the region of steady state increases, which is reflected in Fig. 8(d). When K_{ap} is <0.04 and the bias current ranges from 15 mA to 41 mA, the system is in a steady state, which is represented in blue; $0.04<K_{ap}<0.2$ and the bias current increases from 25 mA to 41 mA, the system is in the period-doubling state, which is marked by green. When the length of the external cavity increases to 6 mm, the region of steady state increases and the period-doubling state reduces, which are reflected in Fig. 8(e).

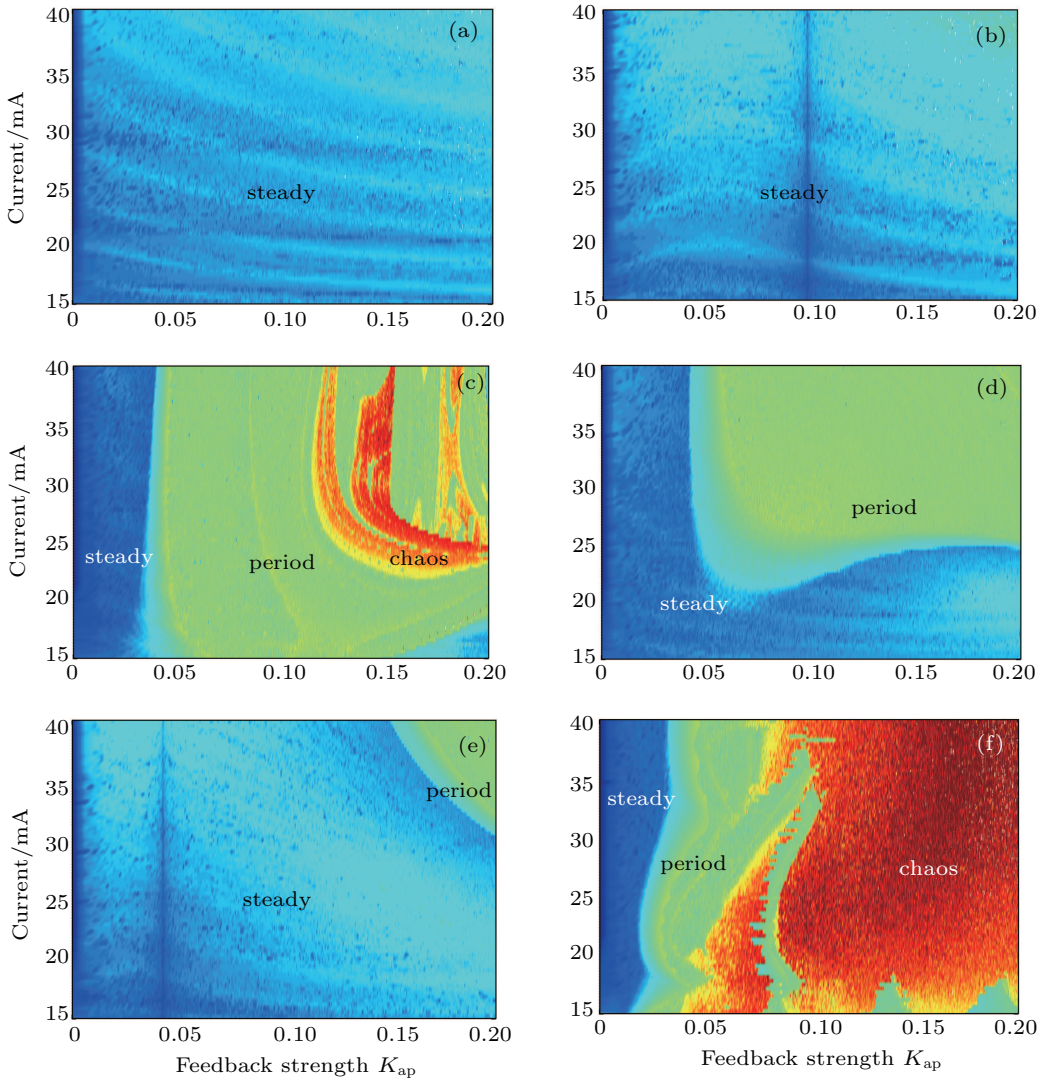


Fig. 8. (color online) Dynamic maps of the chaotic semiconductor laser chip 1 calculated by the largest Lyapunov exponent: (a) $L = 2$ mm, (b) $L = 3$ mm, (c) $L = 4$ mm, (d) $L = 5$ mm, (e) $L = 6$ mm and (f) $L = 4$ cm. The blue represents that the largest Lyapunov exponent is far less than zero; green is near zero; red and yellow are greater than zero.

When $L = 4$ cm, the external cavity frequency f_{ext} is about 3.7 GHz, corresponding to f_r of CSLC1 at 12 mA. As the current increases, f_{ext}/f_r is < 1, which is in the long-cavity regime. It can be seen from the output of CSLC1 in Fig. 8(f), the long cavity is more likely to produce chaos. However, the 4-cm cavity is larger than the butterfly shell and unable to be integrated in a commercial butterfly shell.

Figure 9 shows the numerical result of the largest Lyapunov exponent of CSLC2, where the length of the feedback cavity L is 5 mm and the current $I = 3.33I_{th}$. As shown in Fig. 9, when K_{ap} is less than 0.03, the largest Lyapunov exponent is less than 0, and thus the region is in the steady state; when $0.03 < K_{ap} < 0.08$ and $0.12 < K_{ap} < 0.2$, the largest Lyapunov exponent is around 0, which corresponds to the periodic state; $0.08 < K_{ap} < 0.12$, the largest Lyapunov exponent is greater than 0, and the system is in the chaotic state.

Figure 10 plots the dynamic characteristics of CSLC2. As shown in Figs. 10(a) and 10(b), when the external cavity $L = 2$ mm and 3 mm, the largest Lyapunov exponent remains negative, which is the same phenomenon as CSLC1. However, when the external cavity length increases to 4 mm, the system has no chaotic state, but steady state and periodic state. This is completely different from the dynamic characteristics of the CSLC1, as shown in Fig. 10(c).

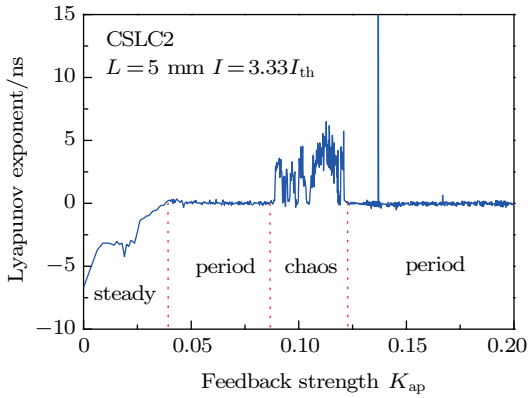


Fig. 9. (color online) Largest Lyapunov exponent as a function of the feedback strength K_{ap} of CSLC2. Feedback cavity $L = 5$ mm and the bias current I is $3.33I_{th}$.

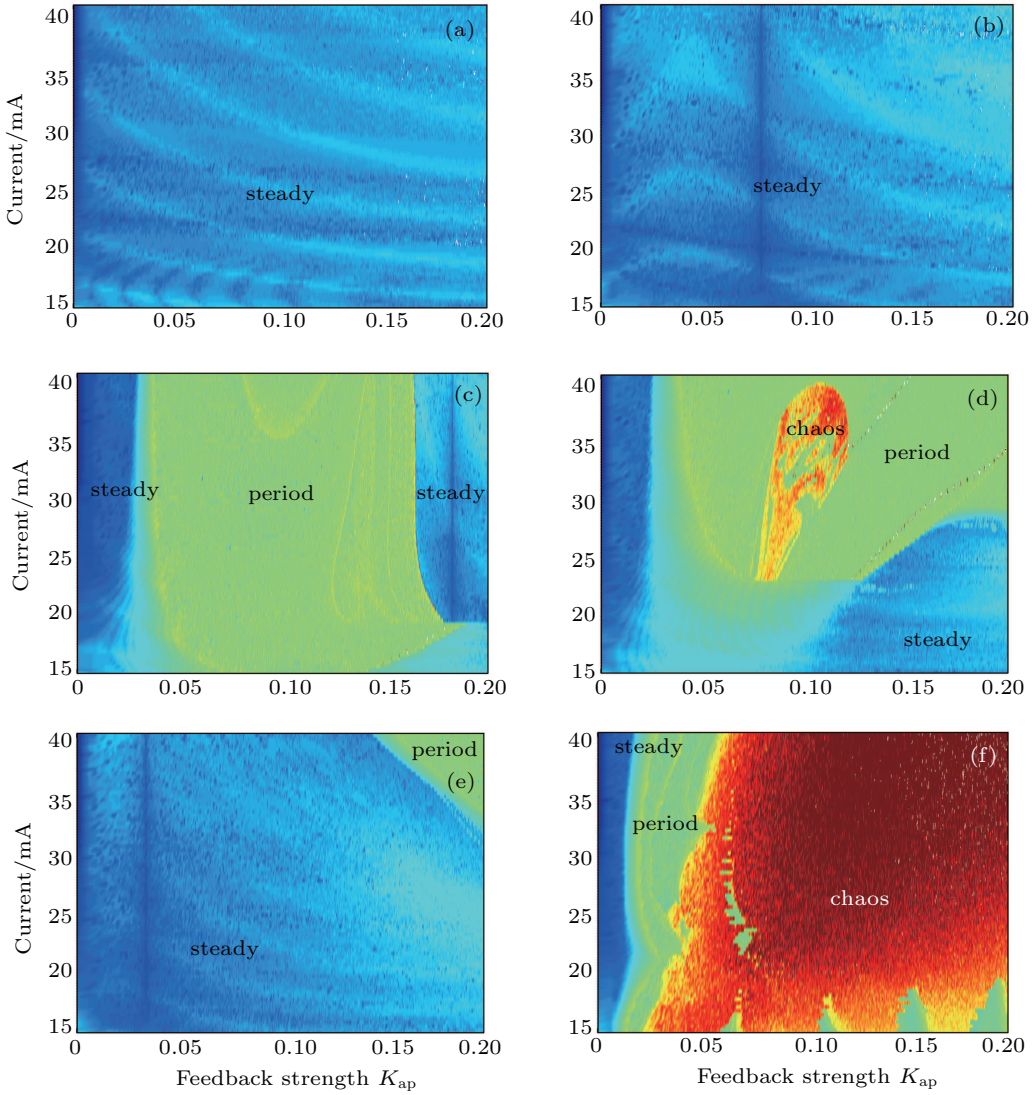


Fig. 10. (color online) Dynamic maps of the chaotic semiconductor laser chip 2 calculated by the largest Lyapunov exponent: (a) $L = 2$ mm, (b) $L = 3$ mm, (c) $L = 4$ mm, (d) $L = 5$ mm, (e) $L = 6$ mm, and (f) $L = 4$ cm. The blue represents that the largest Lyapunov exponent is far less than zero; green is near zero; red and yellow are greater than zero.

When the external cavity length is equal to 5 mm (Fig. 10(d)), the dynamic characteristics of CSLC2 are quite different from those of CSLC1. When $0.07 < K_{ap} < 0.12$ and the bias current is greater than 25 mA, CSLC2 is prone to generate chaos.

When the length of the external cavity increases to 6 mm, the region of steady state increases and the period-doubling state reduces, which are reflected in Fig. 10(e). As the external cavity increases to 4 cm, we also investigate the dynamic characteristics of CSLC2, and the wide regions of chaos can be observed in Fig. 10(f).

The results of this section are obtained by theoretical simulation. We prove the feasibility of this structure by a great mass of theoretical simulations. For a long cavity, we can find that the external-cavity length and the feedback strength have little effect on different chips to generate chaos by comparing the dynamic maps in Figs. 8(f) and 10(f). However, for the regime of short cavity, the optimal external cavity length and feedback intensity are completely different for each chip. We find that the optimal external cavity length and optimal feedback intensity of CSLC1 are $L = 4$ mm and $0.12 < K_{ap} < 0.2$, respectively. The optimal external cavity length and feedback intensity of CSLC2 are $L = 5$ mm and $0.07 < K_{ap} < 0.12$, respectively. Based on this, we must extract the internal parameters of the chips and use them for simulation to obtain the precise production parameters.

The route to chaos of this structure is systematically investigated. The results show that when f_{ext}/f_r is > 5.2, the hybrid integrated chaotic semiconductor laser has a period-doubling route to chaos. We use the maps of the largest Lyapunov exponent to estimate the dynamics of two CSLCs of different external-cavity lengths. The results indicate that the optimal external cavity length and the feedback intensity of CSLC1 are 4 mm and $0.12 < K_{ap} < 0.2$; for CSLC2, the optimal external cavity length and feedback intensity are 5 mm and $0.07 < K_{ap} < 0.12$, respectively. These results indicate that for

the short-cavity structure, the optimal external cavity length and feedback intensity required for each chip to produce chaos are completely different. Therefore, we should extract the internal parameters of the chips and use them for simulation to ensure that the fabricated chaotic laser can generate chaos.

5. Conclusion

We propose a hybrid integrated chaotic semiconductor laser with short-cavity optical feedback. This is a new structure to achieve integration through a simple, low-cost manufacturing process, and it is more conducive to mass production of integrated chaotic semiconductor lasers. To make the simulation results more accurate, we extract the internal parameters of the chaotic semiconductor laser chips (CSLCs) and utilize them for numerical simulation. Based on this method, we can provide accurate external cavity length and feedback intensity for the fabrication of the hybrid integrated chaotic laser and ensure that it can generate chaos. Practically, we have fabricated a hybrid integrated chaotic laser in collaboration with the Institute of Semiconductors of the Chinese Academy of Science.[41] And the experimental phenomena agree well with the theoretical prediction.

We propose the method of combining extraction parameters with numerical simulation for the first time. This study lays a theoretical foundation for the fabrication of hybrid integrated chaotic semiconductor lasers with short-cavity optical feedback.

References

[1] Argyris A, Syvrids D, Larger L, Lodi V A, Colet P, Fischer I, Ojalvo J G, Mirasso C R, Pesquera L and Shore K A 2005 *Nature* **438** 343
[2] Xiang S Y, Wen A J and Pan W 2016 *IEEE Photon. Technol. Lett.* **28** 1988
[3] Kanter I, Aviad Y, Reidler I, Cohen E and Rosenbluh M 2010 *Nat. Photonics Photon.* **4** 58
[4] Li P, Zhang J G, Sang L X, Liu X L, Guo Y Q, Wang A B, Shore K A and Wang Y C 2017 *Opt. Lett.* **42** 2699
[5] Shinohara S, Aenichi A, Davis P, Sunada A and Harayama T 2017 *Opt. Express* **25** 6461
[6] Zhang M J, Ji Y N, Zhang Y N, Wu Y, Xu H and Xu W P 2014 *IEEE Photon. J.* **6** 7902412
[7] Wang L S, Guo Y Y, Li P, Zhao T, Wang Y C and Wang A B 2017 *IEEE Photon. Technol. Lett.* **29** 1723
[8] Ji Y N, Zhang M J, Wang Y C, Wang P, Wang A B, Wu Y, Xu H and Zhang Y N 2014 *Int. J. Bifurcation and Chaos* **24** 1450032
[9] Wang Y C, Wang B J and Wang A B 2008 *IEEE Photon. Technol. Lett.* **20** 1636
[10] Zhao T, Han H, Zhang J G, Liu X L, Chang X M, Wang A B and Wang Y C 2015 *IEEE Photon. J.* **7** 6083909
[11] Xu H, Wang B J, Zhang J G, Han H, Liu L, Wang Y C and Wang A B 2015 *Inc. Microwave Opt. Technol. Lett.* **57** 2502
[12] Gao S L, Zhong S C, Wei K and Ma H 2012 *Acta Phys. Sin.* **61** 180501 (in Chinese)
[13] Li Y, Xu K, Yang B J, Yuan Y and Wu N 2008 *Acta Phys. Sin.* **57** 3353 (in Chinese)
[14] Ma Z, Zhang M J, Liu Y, Bao X Y, Liu H, Zhang Y N and Wang Y C 2015 *IEEE Photon. J.* **7** 6100407
[15] Yi H, Xa L, Xu J, Yu C, Wu Y, Li C and Zhu L 2017 *IEEE Photon. J.* **9** 6803809
[16] Zhang M J, Liu H, Zhang J Z, Liu Y and Liu R X 2017 *IEEE Photon. J.* **9** 1600610
[17] Zhang J Z, Zhang M T, Zhang M J, Liu Y, Feng C K, Wang Y H and Wang Y C 2018 *Opt. Lett.* **43**
[18] Ji Y N, Zhang M J, Wang Y C, Wang P, Wang A B, Wu Y, Xu H and Zhang Y N 2014 *Int. J. Bifurcation and Chaos* **24** 1450032
[19] Yan S L 2016 *Chin. Phys. B* **25** 090504
[20] Yan S L 2014 *Chin. Phys. B* **23** 090503
[21] Sciamanna M and Shore K A 2015 *Nat. Photon.* **9** 151
[22] Dou X, Wu C, Chen X, Yin H, Zhao Q, Hao Y and Zhao N 2014 *Chin. Opt. Lett.* **12** S10610
[23] Yang L, Pan W, Yan L, Luo B, Mu P and Li N 2015 *Chin. Opt. Lett.* **13** 041403
[24] Liu M, Zhang M J, Wang A B, Wang L S, Ji Y N and Ma Z 2013 *Acta Phys. Sin.* **62** 064209 (in Chinese)
[25] Pan B W, Lu D, Yu L Q, Zhang L M and Zhao L J 2015 *Proc. CLEO* **1**
[26] Zhu W Q, Wu Z M, Zhong Z Q, Yin X M, Song J, Zhao L J, Lu D and Xia G Q 2015 *IEEE Photon. Technol. Lett.* **27** 2119
[27] Wu J G, Zhao L J, Wu Z M, Lu D, Tang X, Zhong Z Q and Xia G Q 2013 *Opt. Express* **21** 23358
[28] Sunada S, Harayama T, Arai K, Yoshimura K, Davis P, Tsuzuki K and Uchida A 2011 *Opt. Express* **19** 5713
[29] Yin X M, Zhong Z Q, Zhao L J, Lu D, Qiu H Y, Xia G Q and Wu Z M 2015 *Opt. Commun.* **355** 551
[30] Soriano M C, Garacia-Ojalvo J and Mirasso C R 2013 *Rev. Mod. Phys.* **85** 421
[31] Bosco A K D, Ohara S, Sato N, Akizawa Y, Uchida A, Harayama T and Inubushi M 2017 *IEEE Photon. J.* **9** 6600512
[32] Lang R and Kobayashi K 1980 *IEEE J. Quantum Electron.* **16** 347
[33] Toomey J P, Kane D M, Mcmahon C, Argyris A and Syvridis D 2015 *Opt. Express* **23** 18754
[34] Olshansky R, Hill P, Lanzisera V and Powazinik W 1987 *IEEE J. Quantum Electron* **23** 1410
[35] Morton P A, Tanbun-Ek T, Logan R A, Sergent A M, Sciortino P F and Coblentz D L 1992 *IEEE Photon. Technol. Lett.* **4** 133
[36] Bjerkan L, Royset A, Hafskjaer L and Myhre D 1996 *J. Lightw. Technol.* **14** 839
[37] Cartledge J C and Srinivasan R C 1997 *J. Lightwave Lightw. Technol.* **15** 852
[38] Ye J, Li H and McInerney J G 1993 *Phys. Rev. A* **47** 2249
[39] Ahmed M, Yamada M and Abdulrhmann S 2009 *Int. J. Numer. Model* **22** 434
[40] Lei Y M and Zhang H X 2017 *Chin. Phys. B* **26** 030502
[41] Zhang M J, Xu Y H, Zhao T, Niu Y N, Lv T S, Liu Y, Zhang Z K, Zhang J Z, Wang Y C and Wang A B 2017 *IEEE Photon. Technol. Lett.* **29** 1911